Flexible, Stretchable, and Biodegradable Thin-Film Silicon Photovoltaics

Xing Sheng, Shuodao Wang, and Lan Yin

Abstract This chapter provides an overview of recent progress in the study of thin-film Si photovoltaic (PV) technologies, specifically devices in flexible, stretchable, and/or degradable formats for biomedical applications. First, various approaches for synthesis, fabrication, and assembly of different types of thin-film Si PV cells, ranging from amorphous Si, microcrystalline Si to single-crystalline Si cells, are reviewed. Performances of various cells are also discussed. Materials selection and mechanical considerations are presented, both analytically and numerically, for achieving design flexible and stretchable Si PV cells for lightweight, wearable, and/or implantable light detection and energy harvesting systems. Finally, strategies to form thin-film Si PV cells in a water-soluble and biodegradable "transient" format for bio-integration are discussed. Because of these novel characteristics, thin-film Si PV cells offer a promising solution for energy supply in emerging biomedical applications.

1 Introduction

Silicon (Si)-based solar cells have dominated most of the photovoltaic (PV) market, because of the abundance of Si and the mature technology associated with Si-based semiconductor devices. Si solar cells have achieved wide applications for terrestrial solar energy harvesting, from rooftop mounted solar panels to large utility-scale

X. Sheng (✉)
Department of Electronic Engineering, Tsinghua University, Beijing, China
e-mail: xingsheng@tsinghua.edu.cn

S. Wang
Department of Mechanical and Aerospace Engineering, Oklahoma State University, Stillwater, OK, USA
e-mail: shuodao.wang@okstate.edu

L. Yin
School of Materials Science and Engineering, Tsinghua University, Beijing, China
e-mail: lanyin@tsinghua.edu.cn

S. Ikhmayies (ed.), *Advances in Silicon Solar Cells*,
https://doi.org/10.1007/978-3-319-69703-1_6

solar farms. Compared to their bulk wafer counterparts, thin-film Si cells with thicknesses from tens of micrometers to a few hundred nanometers not only reduce the cell cost by using less material but also offer various attractive features associated with the thin-film device geometry. Advanced materials processes, mechanical design tools, and micro-/nanoelectronic fabrication methods enable us to build thin-film Si PV devices and systems in flexible, stretchable, and/or biodegradable formats. Because of their light weight and compatibility with soft, curvilinear, and/or even wet systems (especially, biological systems), such thin-film Si PV cells provide promising solutions to light detection and power generation for a variety of applications including wearable or implantable biomedical electronic and photonic systems.

2 Strategies of Forming Thin-Film Si PV Cells

In contrast to thick Si wafer-based solar cells that are produced by cutting and sawing process, thin-film Si cell fabrication requires advanced microelectronic processing methods. In addition, those methods should also be compatible with substrate materials that enable flexible and/or stretchable functionalities. In this section, synthesis and fabrication methods for making thin-film Si solar cells, including amorphous Si (a-Si), microcrystalline Si (μc-Si), as well as single-crystalline Si (c-Si), are summarized. The cell performance is also discussed and compared.

2.1 Amorphous and Microcrystalline Si PV Cells

Vacuum-based deposition methods allow us to produce a-Si- and μc-Si-based thin-film single-junction and multi-junction solar cells on various substrates, as illustrated in Fig. 1a. These thin films are usually formed by plasma-enhanced chemical vapor deposition (PECVD) (Fig. 1b) [1]. Gases combining silane (SiH_4) and hydrogen (H_2) are introduced into a vacuum reactor chamber. Gas discharge plasma is initiated by using a voltage bias. Positively charged ions (e.g., SiH_3^+ and H^+) bombard the substrate and create hydrogenerated amorphous silicon (a-Si:H) that is deposited onto the substrate. In this process, the incorporation of hydrogen is crucial since hydrogen passivates dangling bond defects in a-Si by forming Si-H bonds, greatly reducing the defect density. Doping of a-Si:H can be accomplished by introducing gases like phosphine (PH_3) and diborane (B_2H_6) to form n-type and p-type a-Si:H layers, respectively. Therefore, by alternating the dopants, a vertical p-i-n junction can be created as the active device layer. One of the key advantages of using a-Si:H stems from its high optical absorption coefficients in the visible spectral range (10^4–10^5 cm^{-1}). Therefore, an a-Si:H p-i-n junction with a thickness of a few hundreds of nanometers is sufficient to absorb most of the solar energy

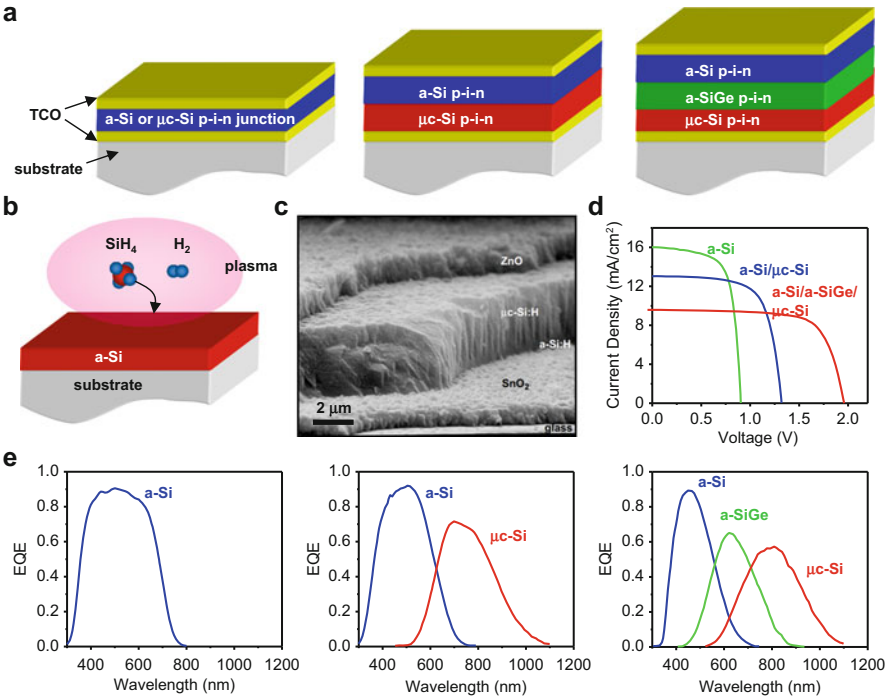

Fig. 1 (**a**) Schematic illustration of thin-film a-Si, a-Si/μc-Si, and a-Si/a-SiGe/μc-Si solar cell structures. (**b**) PECVD process for forming thin-film a-Si. (**c**) SEM image of an a-Si/μc-Si cell [2]. (**d**) Current density–voltage curves for a-Si, a-Si/μc-Si, and a-Si/a-SiGe/μc-Si cells with world-record efficiencies under the AM1.5g spectrum [4–6]. (**e**) External quantum efficiency (EQE) spectra for a-Si, a-Si/μc-Si, and a-Si/a-SiGe/μc-Si cells with world-record efficiencies [4–6] (Reproduced with permission. Copyright 1999 Springer. Copyright 2013 Wiley-VCH. Copyright 2013 Elsevier)

above the optical bandgap of a-Si:H (~1.6 eV). Contact electrodes are fabricated by depositing transparent conductive oxides (TCOs) such as indium tin oxide (ITO), aluminum-doped zinc oxide (AZO), or fluorine-doped tin oxide (FTO). In the PECVD process, the induced plasma enables the film deposition at relatively low temperatures (200–400 °C), which makes the process compatible with various flexible substrates such as metal (stainless steel, aluminum, etc.) and plastic films.

Single-junction a-Si solar cells with a bandgap of about 1.6 eV covers the spectral range from about 300 nm to 800 nm (Fig. 1e). In order to utilize photons with lower energies and achieve higher cell efficiencies, multi-junction cell architectures can be realized by modifying the PECVD process and incorporate other semiconductor junctions. Microcrystalline (μc-Si) solar cells with a bandgap of ~1.1 eV can be formed by varying the PECVD process conditions (plasma frequency, chamber pressure, gas flow rate, etc.), which allow the fabrication of a-Si/μc-Si double-junction "micromorph" cells (Fig. 1a). Figure 1c shows a characteristic cross-sectional scanning electron microscopic (SEM) image of an a-Si/μc-Si

double-junction cell [2]. In addition, germanium (Ge) can be introduced by adding germane (GeH_4) into the gas flow. The formed a-SiGe alloy has a tunable bandgap from 1.6 eV to 0.8 eV by varying the germanium concentration [3]. Therefore, triple-junction a-Si/a-SiGe/μc-Si (1.6 eV / 1.4 eV / 1.1 eV) cells can be fabricated, which cover a wider spectral range from 300 nm to 1100 nm. By adjusting the cell structures (layer thicknesses, surface textures, intermediate layers, etc.), cell performance can be optimized. Figure 1d plots the current–voltage characteristics for the world record a-Si, a-Si/μc-Si, and a-Si/a-SiGe/μc-Si cells under the standard AM1.5 g spectrum [4–6]. By far, maximum 1-sun efficiencies for these a-Si, a-Si/μc-Si, and a-Si/a-SiGe/μc-Si cells are 10.2%, 12.7%, and 13.6%, respectively [7]. Typical spectral responses (external quantum efficiency, EQE) for these a-Si, a-Si/μc-Si, and a-Si/a-SiGe/μc-Si cells are plotted in Fig. 1e [4–6].

2.2 *Single-Crystalline Si PV Cells*

As discussed above, thin-film a-Si-based single- and multi-junction solar cell technologies have been explored for decades and gained great success in various commercial productions, from portable consumer devices to large scale on-grid and off-grid power plant systems [1, 8]. Despite these accomplishments, a-Si- and μc-Si-based thin-film cells still have efficiencies inferior to their single-crystalline (c-Si) counterparts, mostly because of the high defect densities associated with the dangling bonds and grain boundaries. In addition, a-Si-based cells exhibit degradation (Staebler-Wronski effect) due to light-induced metastable defects [1]. Therefore, it is desirable to explore thin-film Si cells in a c-Si format to obtain low-cost, mechanically flexible, and highly efficient modules at the same time. However, it is challenging to fabricate thin-film c-Si devices with a thickness less than 50 μm based on conventional wafer sawing and dicing techniques. In this part, an overview of some very recent progress on the fabrication of thin-film c-Si solar cells using unconventional "kerf-less" methods is provided. These methods enable the isolation of thin-film Si membranes or devices (from tens of nanometers to tens of micrometers thick) from thick Si wafers and all the Si membranes to be integrated with flexible supporting substrates for further uses.

One way to obtain free-standing thin-film Si devices is to start with silicon-on-isolator (SOI) wafer substrates. As illustrated in Fig. 2a, the SiO_2 insulating layer can be selectively removed by hydrofluoric acid (HF)-based wet etching process: $SiO_2 + 6HF \rightarrow 2H_2O + 2H^+ + SiF_6^{2-}$, while the Si top layer and the substrate remain intact. Specific photoresist structures serve as anchors, holding the released devices in suspended forms at their original locations after complete undercut [9]. For example, Fig. 2b shows the SEM image of a completely undercut SOI mesa structure, with photoresist anchor structures underneath the Si [9]. After etching, the unetched Si top layer can be released from the Si substrate and transferred onto various new substrates [10]. Based on this technique, a variety of

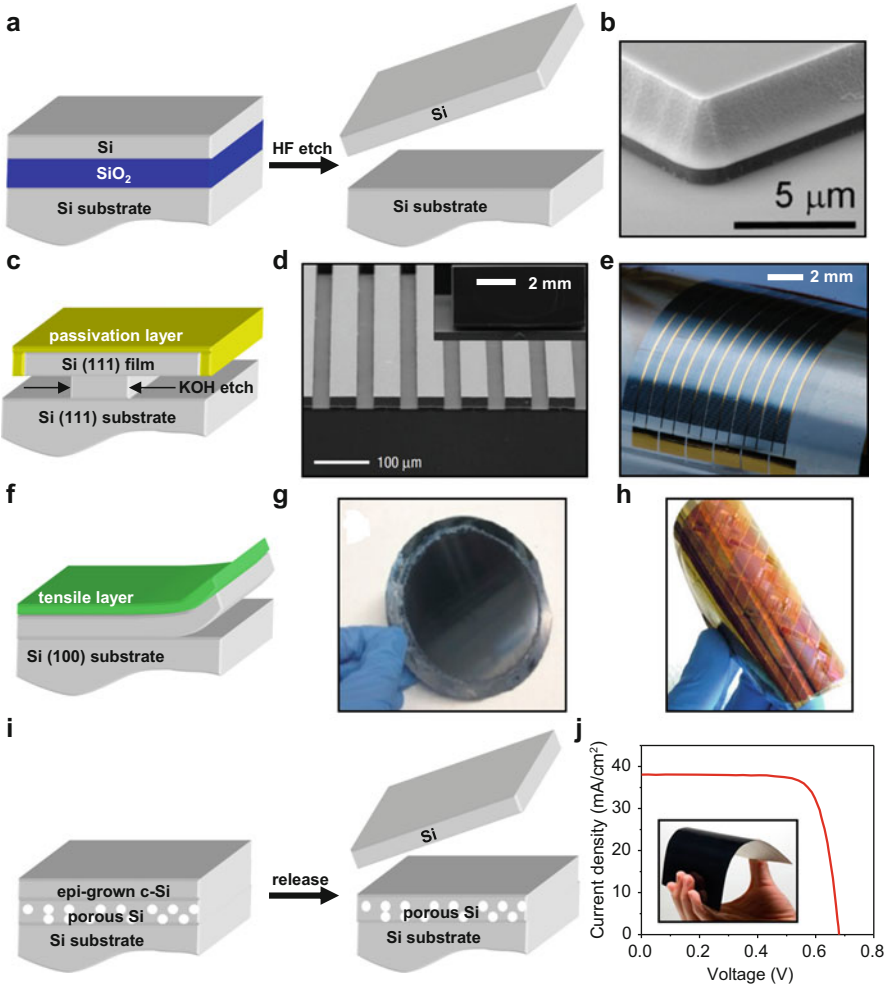

Fig. 2 (**a**) Schematic illustration of releasing a c-Si thin film from a SOI substrate using HF undercut. (**b**) SEM image of a fully HF undercut c-Si film on a SOI substrate, with photoresist anchor structures underneath [9]. (**c**) Schematic illustration of releasing a c-Si thin film from a Si (111) substrate using KOH anisotropic etching. (**d**) SEM image of ribbon-shaped c-Si microcell array on a Si (111) wafer after KOH undercut. Inset: magnified cross-sectional SEM image of a typical c-Si cell, with a thickness of about 20 μm [12]. (**e**) Optical image of an interconnected c-Si microcell array printed on a flexible substrate after KOH undercut [12]. (**f**) Schematic illustration of forming a c-Si layer by controlled spalling process. (**g**) Optical image of exfoliated thin-film Si layers (11 μm thick, 4 inch diameter) [13]. (**h**) Optical image of a flexible c-Si-based circuit (~10 μm thick) by controlled spalling [14]. (**i**) Schematic illustration of releasing an epitaxially grown c-Si layer from an anodic porous Si surface. (**j**) Current density–voltage curves for a representative exfoliated c-Si cells (35 μm thick) under the AM1.5g spectrum [7]. Inset: image of a flexible c-Si cell [16] (Reproduced with permission. Copyright 2012 IOP Publishing. Copyright 2008 Nature Publishing Group. Copyright 2015 Wiley-VCH. Copyright 2013 American Chemical Society)

thin-film c-Si devices with thicknesses from tens of nanometer to tens of micrometers are fabricated and utilized for different applications [11].

In spite of the simple process of creating thin-film c-Si devices using HF undercut SOI substrates, it is impractical to use it for large area PV cell fabrication because of the high cost associated with the SOI wafers. Therefore, it is indispensable to develop alternative processes of directly producing thin-film c-Si materials using thick c-Si wafers, and the wafers can be recycled for multiple uses. Several methods are proposed and demonstrated, as illustrated in Fig. 2c, f, i.

In Fig. 2c, a Si (111) wafer is used as the starting material. Aligned along the [110] direction, ribbon-shaped solar cells are fabricated based on doping, lithographic, and etching processes, with top surfaces and sidewalls protected by a metallic layer. When the wafer is immersed into an alkaline-based (potassium hydroxide, KOH) aqueous solution, the undercut process takes the advantage of the anisotropic etching; the etching rate along the Si [110] direction is 100–1000 times higher than that along the Si [111] direction. Ribbon PV cells with different geometries (thickness, width, and density) can be obtained, allowing the formation of semitransparent and mechanically flexible microcell arrays (Fig. 2e) [12].

Another way to obtain exfoliated c-Si films from Si wafers is to utilize a controlled spalling process (Fig. 2f) [13, 14]. In this process, a metallic layer (e.g., Ni) is coated onto the Si wafer, with a controlled thickness. Internal tensile stress within the coated metal film can be introduced during the deposition process or via the thermal expansion mismatch during annealing. Once a crack is initiated at the wafer edge, the fracture can propagate parallel to the wafer surface direction, creating an exfoliated flexible c-Si layer (Fig. 2g). The thickness of the exfoliated Si layer is controlled by the tensile stress as well as the thickness of the deposited metal film. Assisted by this controlled spalling process, c-Si films with a diameter up to 5 inches have been demonstrated. In addition, this method can also be directly applied on semiconductor ingots, eliminating the wafer sawing process. Figure 2h shows a fabricated Si device array based on the spalling process [14].

In addition, thin-film c-Si device can be formed by epitaxially growth and release c-Si layers from a porous Si surface [15, 16] (Fig. 2i). In this process, a porous Si layer is firstly formed on the Si substrate, usually by Si anodization in HF solution [15]. Subsequently, the anodized Si is used as a growth substrate, on which a c-Si film with a controlled thickness is grown using high-temperature chemical vapor deposition (CVD). After the PV cell fabrication and bonding onto a foreign substrate, the thin-film cell can be separated from the growth wafer by applying a mechanical force at the porous Si layer. The Si wafer can be polished and reused for new cell fabrication. The high-temperature deposition process ensures that the formed c-Si PV cells achieve high crystal and device quality. Based on this porous Si release method, a thin-film flexible c-Si cell (35 μm thick) with a 1-sun efficiency of 21.2% has been demonstrated [7, 16].

3 Flexible and Stretchable Thin-Film Si Solar Cells

By replacing thick, rigid, and hard Si substrates with thin-film Si, one of the key advantages is to achieve mechanically flexible PV cells and modules, since the film flexural rigidity is proportional to the cube of the film thickness [11]. In addition, mechanically stretchable cells and modules can be realized by the combination of material and mechanical design methods. In this section, material requirements and mechanical designs for device integration to obtain flexible and stretchable thin-film Si PV cells and modules are presented. Potential applications for flexible and stretchable cells are discussed.

3.1 Substrate Requirements and Applications

Unlike conventional thin-film PV cells that are formed onto thick glass or metal substrates, flexible and/or stretchable cells require thin metal or polymer substrates to obtain desired mechanical properties. For a-Si-based single- and multi-junction cells, the deposition process (PECVD) requires that cell substrates remain stable at elevated temperatures (200–400 °C), as discussed previously. Cell fabrication has been realized on substrates made by materials like stainless steel and polyimide, as shown in Fig. 3a, b, respectively. In addition, flexible substrates enable the roll-to-roll cell production, greatly enhancing the process speed and reducing the cost. By using the roll-to-roll process, PV modules with areas of few square meters can be formed, with efficiencies up to 12% [7]. Compared to cells on rigid substrates, large area flexible PV modules have advantages in transportation and installation and are more compatible with building integrated power systems (Fig. 3d). Small area PV cells can be mounted onto wearable and portable systems like back bags, clothes, and cellphones (Fig. 3e) and even onto the surface of human skin (Fig. 3f), working as power sources for both military and civilian uses.

The use of thin-film Si layer release and transfer processes that further expands candidate materials that can be explored as thin-film cell substrates, because the cell process can be performed at room temperature. Flexible thin-film c-Si cells laminated on transparent polymer substrates have shown efficiencies of more than 21% [7]. Furthermore, thin-film c-Si cells integrated onto elastomer-based substrates (e.g., silicones) can achieve both mechanical flexibility and stretchability, making it more compatible with biological systems such as soft human tissues. For example, Fig. 3c illustrates a c-Si photodiode array printed onto polydimethylsiloxane (PDMS)-based substrates [17]. The unusual materials and mechanical design ensure that the device can be elongated by more than 20% without mechanical fracture. With careful designs, such thin-film microscale solar cells can be integrated within the epidermal electronic circuit systems (Fig. 3f), serving as a wireless power source for various electronic and photonic skin-mounted biological sensors [18].

Fig. 3 (**a**) Photograph of flexible a-Si solar cells deposited onto stainless steel substrates, prepared by roll-to-roll process [19]. (**b**) Optical image of a flexible Si solar cell printed on a glass window surface [20]. (**c**) Optical image of c-Si photodiode arrays printed onto PDMS substrates [17]. (**d**) Photograph of flexible a-Si solar modules for building integration [19]. (**e**) Flexible solar cells mounted on a portable device [20]. (**f**) Optical image of epidermal electronic circuits (Reproduced with permission. Copyright 2008 Wiley-VCH. Copyright 2012 Nature Publishing Group. Copyright 2008 PNAS)

3.2 Mechanical Considerations

Silicon is an extremely brittle material which breaks when stretched by less than 1% of strain; therefore careful designs are required to overcome this intrinsic mechanical limit. This is especially challenging when the fabrication and processing involve the integration of mechanically dissimilar materials such as in the stretchable and flexible systems shown in Figs. 2e, h and 3. The key strategy in realizing these systems is to design these composite structures such that large deformation occurs in the elastomeric materials while the brittle components barely deform. Many advanced mechanics ideas and fabrication processes have been developed for a wide range of applications based on stretchable inorganic electronics, represented by the work of Ko et al. [21], Baca et al. [12], and Kim et al. [18]. Many of these mechanics analyses can be adapted for the designs of flexible and stretchable PV systems due to the similarities in materials and geometric layouts.

Here we limit our discussions on designs and mechanics specifically related to PV applications with the example shown in Fig. 2e. This flexible PV module involves a composite structure consisting of a planarizing/adhesive layer (NOA61; thickness ~ 30 μm), which also serves as the substrate, arrays of μ-cells

and metal interconnects, and a polymer encapsulation layer (NOA61; thickness ~ 30 μm). The mechanically flexible μ-cell module is modeled as a composite beam as shown in Fig. 4a, where W, W_{Si}, and W_{NOA} are the widths of the beam, silicon μ-cell, and the distance between adjacent μ-cells, respectively, and t, t_m, b, and $(a\text{-}t)$ are the thicknesses of the μ-cell, metal interconnect layer, and NOA layers above and below the μ-cell. The Young's modulus of silicon, metal (Au), and NOA are denoted by E_{Si}, E_{Au}, and E_{NOA}, respectively. The strain in the beam is given by $\varepsilon_{yy} = (z - z_0)/R$, where R is the bending radius of the beam and z_0 is the position of the neutral mechanical plane measured from the bottom edge. Using the geometric and material parameters shown in Fig. 4a, z_0 is obtained analytically by

$$z_0 = \frac{a-t}{2}\left(1+\frac{b}{a-t}\right)^2 + 2\frac{b}{a-t}\frac{t+t_m}{a-t} + \frac{W_{NOA}}{W}\frac{t}{a-t}\left(2+\frac{t}{a-t}\right) + \frac{E_{Si}t}{E_{NOA}(a-t)}\frac{W_{Si}}{W}\left(2+\frac{t}{a-t}\right) + \frac{E_{Au}t_m}{E_{NOA}(a-t)}\left(2+\frac{2t+t_m}{a-t}\right)1+\frac{b}{a-t} + \frac{W_{NOA}}{W}\frac{t}{a-t} + \frac{E_{Si}t}{E_{NOA}(a-t)}\frac{W_{Si}}{W} + \frac{E_{Au}t_m}{E_{NOA}(a-t)}. \quad (1)$$

The above analytical modeling can be used to tune the geometric layout (especially the thicknesses of different materials) such that the neutral mechanical plane is placed near the center of the Si μ-cells, which then ensures the maximum strains in the silicon and metal interconnects remain small even when the entire structure undergoes extreme deformation. For the experimental data shown in Fig. 4b, the above equations predict that the strain in the silicon is less than 0.3% even for severe bend radii less than 5 mm, for bending in any direction. Finite element modeling, with representative results shown in Fig. 4c, d, confirms that the maximum strain in silicon for the inward and outward bending is around 0.03%, and the maximum strain in the metal layer is around 0.13%, located near the silicon corner for both inward and outward bending as shown in Fig. 4d. Module performance, evaluated in outward bending along and perpendicular to the cell length under AM1.5 g illumination, shows behaviors consistent with expectations on the basis of mechanics analysis and relative insensitivity of the degree of illumination across the modest area of the module, for the bend radii examined here. For example, at bending radii of 12.6, 8.9, 6.3, and 4.9 mm, the module efficiency (~ 6.0%) and fill factor (~ 0.60) remain unchanged as summarized in Fig. 4e, f. The small strain in active device components not only ensures consistent module performance but also prevents fracture when these systems are used in environments that impose repetitive loadings. Fatigue tests, with bending up to 200 cycles, also show little change in performance, as summarized in Fig. 4g.

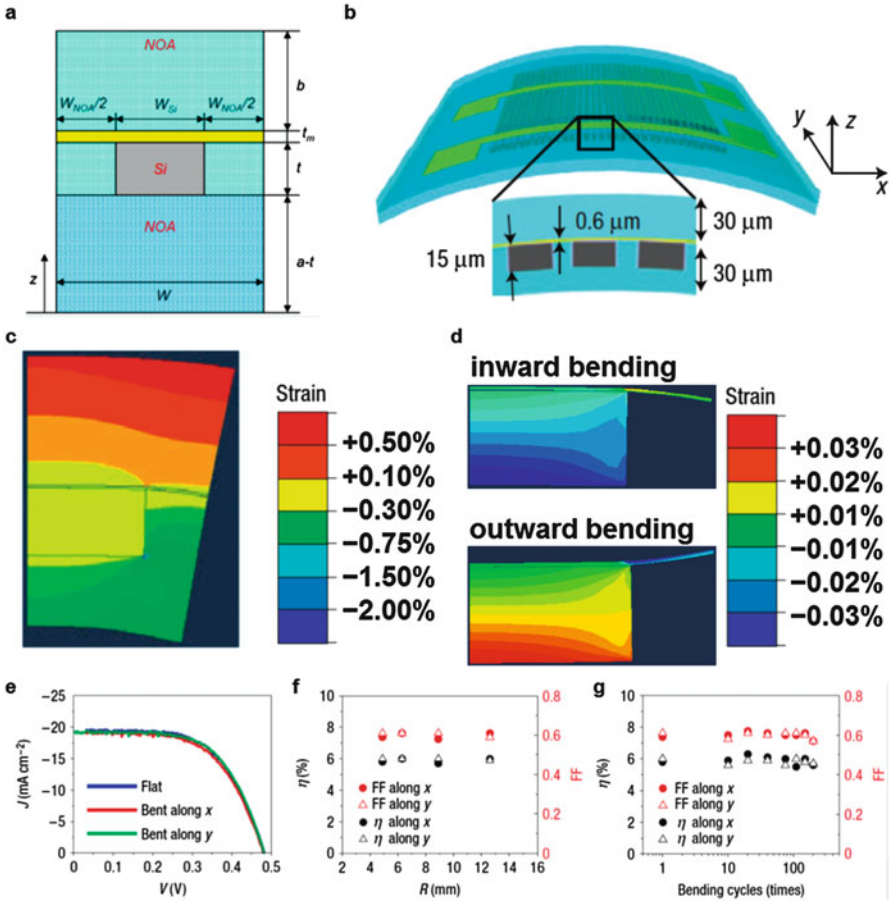

Fig. 4 (**a**) Cross-sectional schematic illustration of a model composite structure composed of silicon μ-cell, and polymer encapsulation layer and a metal layer. (**b**) Schematic illustration of an optimized design in which the neutral mechanical plane is positioned near the center of the μ-cells (gray) through judicious choices of thickness for the polymer (blue) substrate and overcoat. (**c**) Color contour plot of calculated bending strains through the cross-section of a mechanically flexible μ-cell module, bent along the cell width direction at $R = 4.9$ mm. The calculations use symmetry boundary conditions for evaluation of a single unit cell of the system. The black lines delineate the boundaries of the μ-cell and metal interconnect line (top). (**d**) Color contour plot of calculated bending strains through the cross-section of a mechanically flexible μ-cell module, bent inward and outward along the cell width direction at $R = 4.9$ mm, without metal layer. (**e**) *J*–*V* data from a module under AM1.5 g illumination in a flat configuration and bent along the cell width (x) and length (y) directions, both for $R = 4.9$ mm. (**f**) Plot of η and fill factor (FF) under AM1.5 g illumination for $R = 12.6$, 8.9, 6.3, and 4.9 mm. (**g**) Plot of η and FF as a function of bending cycles up to 200 times at $R = 4.9$ mm [12] (Reproduced with permission. Copyright 2008 Nature Publishing Group)

4 Biodegradable Thin-Film Si Photovoltaic Cells

Recently, bio-integrated electronic and optical devices that can dissolve naturally in physiological conditions have attracted considerable attentions because of their potential applications in biomedical surgery, diagnosis, and therapy [22–27]. Comprising fully biodegradable materials (metals [25, 26], semiconductors [27, 28], dielectrics [29], and polymers [30, 31]), implantable devices dissolve in biological environments in a controlled manner after use. Such devices and systems are of particular interest since they eliminate the risk of secondary surgery after implantation. The operation of these systems also requires fully dissolvable energy devices as a power supply. In this section, we summarize some of the recent progress about the development of fully degradable thin-film Si photovoltaic cells, which provide a promising solution for remote and wireless powered energy source for these biodegradable and implantable electronic and photonic devices.

4.1 Materials Degradation

The hydrolysis process of thin-film Si materials can be simply described as the reaction of Si with water to form silicic acid: $Si + 4H_2O \rightarrow Si(OH)_4 + 2H_2$, in which the Si dissolution rate varies with lots of factors like the Si crystallinity, doping, pH levels, temperature, and the solution chemistry [28]. Figure 5a plots the dissolution rates of monocrystalline Si (c-Si), polycrystalline Si (poly-Si), and amorphous Si (a-Si) in buffer solutions with different pH levels (pH 6, pH 7, pH 7.4, pH 8, and pH 10) at physiological temperature (37 °C) [23, 27]. In these experiments, c-Si thin-film membranes are prepared by transfer printing process, while poly-Si and a-Si layers are formed by chemical vapor deposition (CVD) methods. Dissolution rates range from about 1 nm/day to about 1 nm/sec, depending on pH levels in the solution. Additional details about dissolution for Si with different doping levels in different physiological environments (deionized water, phosphate-buffered saline, bovine serum, etc.) have also been extensively studied [28]. As an example, the dissolution process of a c-Si membrane in bovine serum (pH 7.4) at 37 °C is presented as the evolution of atomic force microscopic (AFM) images in Fig. 5b [28]. Dissolution behaviors of biodegradable metals (Mg, Fe, Zn, Mo, W, etc.), dielectric materials (ZnO, SiO_2, Si_3N_4, etc.), and polymers (silk, PLGA, PLA, etc.) are also investigated and discussed [25–31]. Combining these materials with Si-based junctions, thin-film Si PV cells can be formed in a fully degradable format. Figure 5c illustrates the functional transience of such a degradable solar cell during hydrolysis, made from an a-Si:H pn junction with ZnO- and Mg-based contacts [27]. Structural evolution for the a-Si:H solar cell is shown in Fig. 5d [27]. It is observed that the Mg and ZnO contacts dissolve within a few hours in water, followed by the destruction of the a-Si:H layer. Complete dissolution of the rest a-Si:H material occurs after several days.

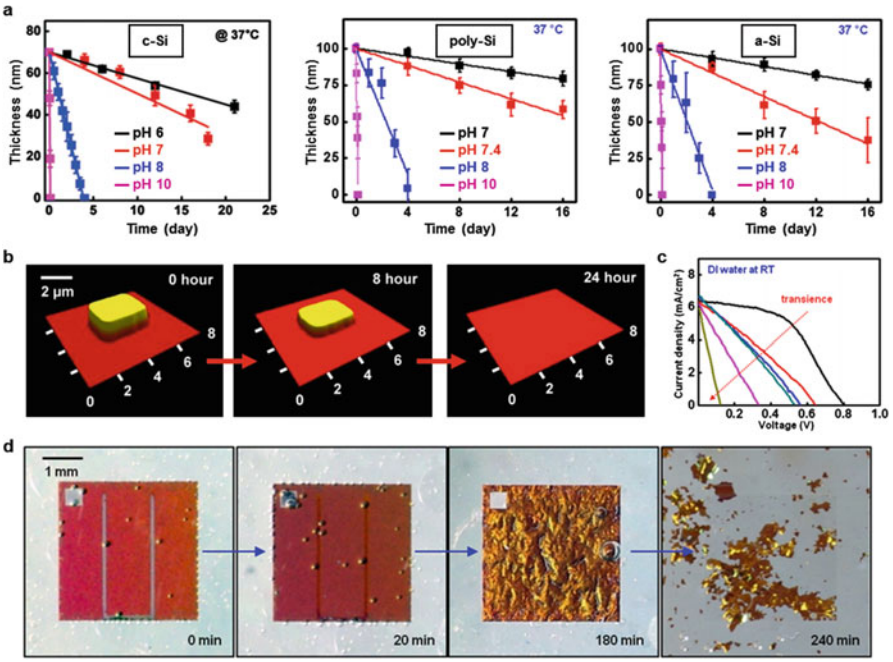

Fig. 5 (**a**) Theoretical (lines) and experimental (symbols) dissolution rates for different types of thin-film Si (c-Si, poly-Si, and a-Si) in buffer solutions with different pH at physiological temperature (37 °C) [23, 27]. (**b**) AFM images of a c-Si thin-film layer at various dissolution stages at pH of 7.4 [28]. (**c**) IV characteristics and performance degradation of a thin-film a-Si:H solar cell, made by fully degradable materials [27]. (**d**) Optical images showing the dissolution of a thin-film a-Si:H solar cell in deionized water at room temperature [27] (Reproduced with permission. Copyright 2014 Wiley-VCH. Copyright 2015 American Chemical Society. Copyright 2014 American Chemical Society)

4.2 Biological Compatibility

In order to evaluate the biocompatibility of these biodegradable electronic devices and ultimately use them for implantable biomedical applications, in vitro and in vivo cytotoxicity tests are necessary. Fluorescence images in Fig. 6a show the viability of L929 mouse fibroblast cell lines cultured on the surface of poly-Si thin films [27]. Results show that the cell viability reaches more than 95% after 7 days. Similar results are obtained for cells grown on other semiconductor surfaces including a-Si, SiGe, Ge, and mono-Si, summarized in Fig. 6b [27]. Cell culture studies on other materials like SiO_2 are also explored in previous works [29]. Furthermore, the constituent materials (e.g., Si, Mg, Zn, etc.) used to form the thin-film PV cells have been proved to be biocompatible, with the amounts far below the daily intake limits for clinical use [22, 25]. To demonstrate the biocompatibility for those thin-film Si-based devices, a representative device array of thin-film Si

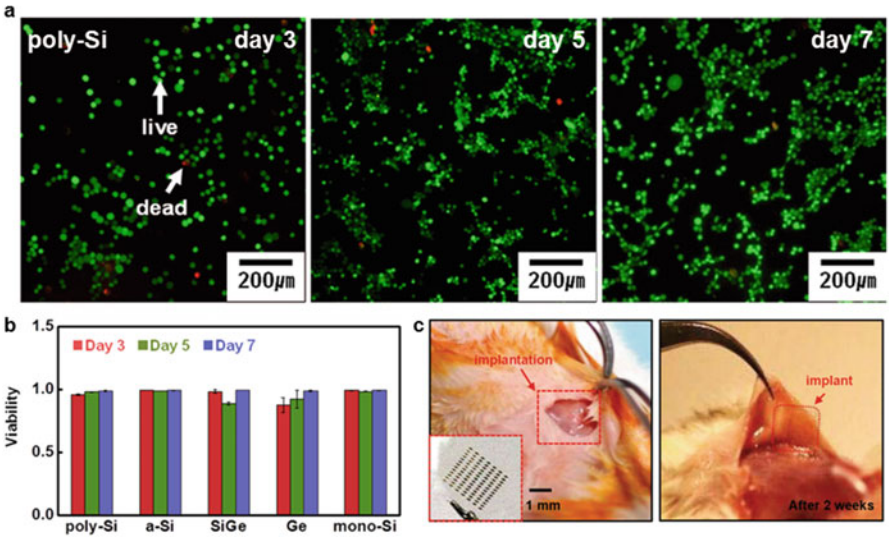

Fig. 6 (**a**) Fluorescence images illustrating cell viability on a poly-Si thin film, where live and dead cell assays are labeled as green and red, respectively [27]. (**b**) Viability for cells cultured on surfaces of poly-Si, a-Si, SiGe, Ge, and mono-Si at day 3, day 5, and day 7 [27]. (**c**) In vivo demonstration of a thin-film c-Si electronic device array implanted in the dorsal region of a mouse. The devices disappear in 3 weeks after the surgery [24] (Reproduced with permission. Copyright 2015 American Chemical Society. Copyright 2013 Wiley-VCH)

CMOS transistors (with Mg contacts) on silk substrates is implanted underneath the skin of a living mouse (Fig. 6c). The implanted region is examined after 2 weeks, revealing that the device array has fully degraded and absorbed by biological tissues [24].

Additional considerations for the use of implantable Si PV cells include the optical effects of biological tissues (skin, skull, fat, etc.) and the solar cell device optimization. Unlike solar cells working directly under the sun, the implantable devices are only operational within the transparency window of the biological tissue, which is usually in the red and near-infrared spectral range. At these wavelengths, thin-film Si PV cells usually have low efficiencies due to low absorption coefficients. Therefore, the Si film thickness should be optimized to obtain a trade-off among power generation, dissolution time, and mechanical flexibility. In such thin-film Si PV cells, light-trapping schemes could be adapted to optimize the cell optical absorption in the red and near-IR range [32]. In addition, advanced encapsulation and packaging strategies can be implemented to realize a more controllable degradation process. These full degradable thin-film Si PV cells provide a viable and promising approach to realize the wireless energy transfer for implantable biomedical systems, with potential applications including drug delivery [31], optogenetic stimulation [33], temperature monitoring [34], etc.

5 Conclusions

In this chapter, it is shown that advanced thin-film Si PV cells not only provide a viable solution for large scale solar energy utilization but also foreshadow a promising future in healthcare applications. Some of the recent progress about advanced thin-film Si solar cells is overviewed, with specific foci on their flexible, stretchable, and biodegradable formats and the associated fabrication schemes. These advanced cell technologies envision new possibilities in broad biomedical applications for wearable and implantable systems. In the future, fundamental research efforts will likely focus on the developments of high-yield and cost-effective approaches to make high-efficiency thin-film c-Si cells that reach thermodynamic efficiency limits for Si cells (one sun efficiency ~ 25%) [32]. Contacting and substrate materials that provide mechanical flexibility and/or biocompatibility are also to be explored, combined with advanced mechanical design strategies. Furthermore, advanced integration schemes need to be investigated to interconnect the thin-film Si PV cells with other electronic components and circuits, like batteries, antennas, transistors, and various sensors, to form a fully functional biomedical device system for sensing, diagnosis, and therapy.

References

1. R.E.I. Schropp, M. Zeman, *Amorphous and Microcrystalline Silicon Solar Cells: Modeling, Materials and Device Technology* (Kluwer Academic Publishers, Boston, 1998)
2. H. Keppner, J. Meier, P. Torres, D. Fischer, A. Shah, Appl. Phys. A Mater. Sci. Process **69**, 169 (1999)
3. C.C. Wang, C.Y. Liu, S.Y. Lien, K.W. Weng, J.J. Huang, C.F. Chen, D.S. Wuu, Curr. Appl. Phys. **11**, S50 (2011)
4. T. Matsui, H. Sai, T. Suezaki, M. Matsumoto, K. Saito, I. Yoshida, M. Kondo, in *Proceedings of the 28th European Photovoltaic Solar Energy Conference and Exhibition*, 2013, p. 2213
5. T. Matsui, H. Sai, K. Saito, M. Kondo, Prog. Photovolt. Res. Appl. **21**, 1363 (2013)
6. S. Kim, J.W. Chung, H. Lee, J. Park, Y. Heo, H.M. Lee, Sol. Energy Mater. Sol. Cells **119**, 26 (2013)
7. M.A. Green, K. Emery, Y. Hishikawa, W. Warta, E.D. Dunlop, Prog. Photovolt. Res. Appl. **23**, 805 (2015)
8. J. Poortmans, V. Arkhipov, *Thin Film Solar Cells Fabrication, Characterization and Applications* (Wiley, Chichester, 2006)
9. H. Keum, A. Carlson, H. Ning, A. Mihi, J.D. Eisenhaure, P.V. Braun, J.A. Rogers, S. Kim, J. Micromech. Microeng. **22**, 055018 (2012)
10. A. Carlson, A.M. Bowen, Y. Huang, R.G. Nuzzo, J.A. Rogers, Adv. Mater. **24**, 5284 (2012)
11. J.A. Rogers, M.G. Lagally, R.G. Nuzzo, Nature **477**, 45 (2011)
12. J. Yoon, A.J. Baca, S.I. Park, P. Elvikiss, J.B. Geddes, L. Li, R.H. Kim, J. Xiao, S. Wang, T.H. Kim, M.J. Motala, B.Y. Ahn, E.B. Duoss, J.A. Lewis, R.G. Nuzzo, P.M. Ferreira, Y. Huang, A. Rockett, J.A. Rogers, Nat. Mater. **7**, 907 (2008)
13. S. Wang, B.D. Weil, Y. Li, K.X. Wang, E. Garnett, S. Fan, Y. Cui, Nano Lett **13**, 4393 (2013)
14. D. Shahrjerdi, S.W. Bedell, Nano Lett. **13**, 315 (2013)

15. H.S. Radhakrishnan, R. Martini, V. Depauw, K. Van Nieuwenhuysen, M. Debucquoy, J. Govaerts, I. Gordon, R. Mertens, J. Poortmans, IEEE J. Photovoltaics **4**, 70 (2014)
16. M.M. Moslehi, Thin-silicon, low-cost solar photovoltaic modules using kerfless epitaxial silicon lift-off technology. Solexel Inc (2012)
17. D.H. Kim, J. Song, W.M. Choi, H.S. Kim, R.H. Kim, Z. Liu, Y. Huang, K.C. Hwang, Y. Zhang, J.A. Rogers, Proc. Natl. Acad. Sci. **105**, 18675 (2008)
18. D.H. Kim, N. Lu, R. Ma, Y.S. Kim, R.H. Kim, S. Wang, J. Wu, S.M. Won, H. Tao, A. Islam, K.J. Yu, T. Kim, R. Chowdhury, M. Ying, L. Xu, M. Li, H.J. Chung, H. Keum, M. McCormick, P. Liu, Y. Zhang, F.G. Omenetto, Y. Huang, T. Coleman, J.A. Rogers, Science **333**, 838 (2011)
19. M. Pagliaro, G. Palmisano, R. Ciriminna, *Flexible Solar Cells* (Wiley-VCH Verlag GmbH & Co. KGaA, Weinheim, 2008)
20. C.H. Lee, D.R. Kim, I.S. Cho, N. William, Q. Wang, X. Zheng, Sci. Rep. **2**, 1000 (2012)
21. H.C. Ko, M.P. Stoykovich, J. Song, V. Malyarchuk, W.M. Choi, C.-J. Yu, J.B. Geddes III, J. Xiao, S. Wang, Y. Huang, J.A. Rogers, Nature **454**, 748 (2008)
22. S.W. Hwang, H. Tao, D.H. Kim, H. Cheng, J.K. Song, E. Rill, M.A. Brenckle, B. Panilaitis, S.M. Won, Y.S. Kim, Y.M. Song, K.J. Yu, A. Ameen, R. Li, Y. Su, M. Yang, D.L. Kaplan, M.R. Zakin, M.J. Slepian, Y. Huang, F.G. Omenetto, J.A. Rogers, Science **337**, 1640 (2012)
23. S.W. Hwang, G. Park, H. Cheng, J.K. Song, S.K. Kang, L. Yin, J.H. Kim, F.G. Omenetto, Y. Huang, K.M. Lee, J.A. Rogers, Adv. Mater. **26**, 1992 (2014)
24. S.W. Hwang, D.H. Kim, H. Tao, T.I. Kim, S. Kim, K.J. Yu, B. Panilaitis, J.W. Jeong, J.K. Song, F.G. Omenetto, J.A. Rogers, Adv. Funct. Mater. **23**, 4087 (2013)
25. L. Yin, H. Cheng, S. Mao, R. Haasch, Y. Liu, X. Xie, S.W. Hwang, H. Jain, S.K. Kang, Y. Su, R. Li, Y. Huang, J.A. Rogers, Adv. Funct. Mater. **24**, 645 (2014)
26. S.K. Kang, S.W. Hwang, S. Yu, J.H. Seo, E.A. Corbin, J. Shin, D.S. Wie, R. Bashir, Z. Ma, J.A. Rogers, Adv. Funct. Mater. **25**, 1789 (2015)
27. S.K. Kang, G. Park, K. Kim, S.W. Hwang, H. Cheng, J. Shin, S. Chung, M. Kim, L. Yin, J.C. Lee, K.M. Lee, J.A. Rogers, ACS Appl. Mater. Interfaces **7**, 9297 (2015)
28. S.W. Hwang, G. Park, C. Edwards, E.A. Corbin, S.K. Kang, H. Cheng, J.K. Song, J.H. Kim, S. Yu, J. Ng, J.E. Lee, J. Kim, C. Yee, B. Bhaduri, Y. Su, F.G. Omennetto, Y. Huang, R. Bashir, L. Goddard, G. Popescu, K.M. Lee, J.A. Rogers, ACS Nano **8**, 5843 (2014)
29. S.K. Kang, S.W. Hwang, H. Cheng, S. Yu, B.H. Kim, J.H. Kim, Y. Huang, J.A. Rogers, Adv. Funct. Mater. **24**, 4427 (2014)
30. H.L. Hernandez, S.K. Kang, O.P. Lee, S.W. Hwang, J.A. Kaitz, B. Inci, C.W. Park, S. Chung, N.R. Sottos, J.S. Moore, J.A. Rogers, S.R. White, Adv. Mater. **26**, 7637 (2014)
31. H. Tao, S.W. Hwang, B. Marelli, B. An, J.E. Moreau, M. Yang, M.A. Brenckle, S. Kim, D.L. Kaplan, J.A. Rogers, F.G. Omenetto, Proc. Natl. Acad. Sci. **111**, 17385 (2014)
32. X. Sheng, L.Z. Broderick, L.C. Kimerling, Opt. Commun. **314**, 41 (2014)
33. T.I. Kim, J.G. McCall, Y.H. Jung, X. Huang, E.R. Siuda, Y. Li, J. Song, Y.M. Song, H.A. Pao, R.H. Kim, C. Lu, S.D. Lee, I.S. Song, G. Shin, R. Al-Hasani, S. Kim, M.P. Tan, Y. Huang, F.G. Omenetto, J.A. Rogers, M.R. Bruchas, Science **340**, 211 (2013)
34. R.C. Webb, A.P. Bonifas, A. Behnaz, Y. Zhang, K.J. Yu, H. Cheng, M. Shi, Z. Bian, Z. Liu, Y.S. Kim, W.H. Yeo, J.S. Park, J. Song, Y. Li, Y. Huang, A.M. Gorbach, J.A. Rogers, Nat. Mater. **12**, 938 (2013)